

NOTE

Anisotropic photon migration in human skeletal muscle

T Binzoni^{1,2}, C Courvoisier³, R Giust³, G Tribillon³, T Gharbi³,
J C Hebden⁴, T S Leung⁴, J Roux⁵ and D T Delpy⁴

¹ Département de Neurosciences Fondamentales, University of Geneva, Switzerland

² Department of Radiology, University Hospital, Geneva, Switzerland

³ Département d'optique PM Duffieux, Institut FEMTO-ST, UMR CNRS 6174,
Université de Franche Comté, Besançon, France

⁴ Department of Medical Physics and Bioengineering, University College London, UK

⁵ Hamamatsu Photonics, Grenoble, France

E-mail: Tiziano.Binzoni@medecine.unige.ch

Received 8 November 2005, in final form 14 December 2005

Published 15 February 2006

Online at stacks.iop.org/PMB/51/N79

Abstract

It is demonstrated in the short head of the human *biceps brachii* of 16 healthy subjects (12 males and 4 females) that near infrared photon migration is anisotropic. The probability for a photon to travel along the direction of the muscle fibres is higher (~ 0.4) than that of travelling along a perpendicular axis (~ 0.3) while in the adipose tissue the probability is the same (~ 0.33) in all directions. Considering that the muscle fibre orientation is different depending on the type of muscle considered, and that inside a given skeletal muscle the orientation may change, the present findings in part might explain the intrasubject variability observed in the physiological parameters measured by near infrared spectroscopy techniques. In other words, the observed regional differences might not only be physiological differences but also optical artefacts.

(Some figures in this article are in colour only in the electronic version)

1. Introduction

Near infrared spectroscopy (NIRS) is one of the techniques of choice allowing one to investigate, non-invasively, the energy metabolism of human skeletal muscle (Ferrari *et al* 1997, 2004). In particular, NIRS appears to be a unique method of measurement in situations where only local metabolic changes are under study, such as could be the case for induced temperature changes in a small region of muscle (Binzoni *et al* 2002). In this respect, the precise assessment of the optical parameters such as the absorption coefficient (μ_a), the

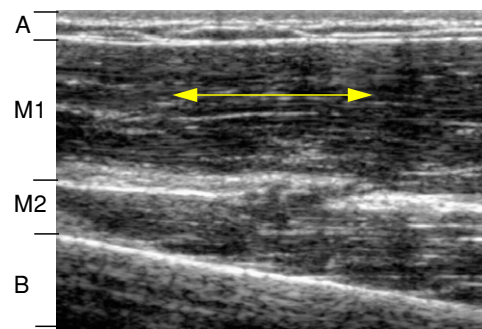


Figure 1. Longitudinal ultrasound image of a human right biceps (cross section along the *humerus* direction); A: skin (comprising the epidermis, the dermis and the hypodermis). The thickness of A is defined for simplicity in the text as adipose tissue thickness (ATT). M1: short head of the *biceps brachii*; M2: *brachialis*; B: *humerus*.

transport-corrected scattering coefficient (μ'_s) of the muscle, etc, is an essential issue, because these parameters are usually used to derive important physiological quantities such as the blood oxygen saturation, the deoxyhaemoglobin concentration, etc. Thus, over the years, numerous mathematical models of light transport in tissue have been developed enabling one to estimate μ_a and μ'_s (in relative or absolute units) from experimental data obtained with different types of NIR spectrometers (e.g. continuous intensity, time-resolved or intensity modulated instruments (Delpy and Cope 1997)). These models can describe in a very precise manner the transport of light in tissue by taking into account for example μ_a , μ'_s , tissue geometry, refractive indices, optical anisotropies, etc (e.g. Arridge *et al* (1992), Martelli *et al* (2002), Dudko *et al* (2004)). However, when it comes to the reported experimental studies on human skeletal muscle, it is apparent that although all these points may have been carefully taken into account, in practice, the assumption has always been made that the muscle is optically isotropic. Since it is clear that optical anisotropy will influence the estimation of physiological parameters, the studies reported have been undertaken to identify the magnitude of these effects.

If one observes the morphological structure of a skeletal muscle, it clearly has an ordered macroscopic structure. Figure 1 shows a longitudinal cross section (along the *humerus* direction), obtained by ultrasonography, of the short head of a human right *biceps brachii*. The arrow identifies the mean direction of the ‘black and white’ striations appearing in the image at the level of the *biceps brachii* (zone labelled as M1). These striations are generated by the presence of fascicles of muscle fibres, all going in the same direction, interacting with the ultrasound waves. Thus, this image clearly shows that, from the morphological point of view, the macroscopic structure of skeletal muscle is not isotropic. This ‘striated’ structure is found by definition in all human skeletal muscles. It is known that at a microscopic level the orientation of muscle fibres affects the optical properties (Zijp and ter Bosch 1998, Marchesini 1999). However, it is not known if such anisotropic effects are still observable when measurements are made over large distances (e.g. optode separations of ~ 3 cm) and through overlying tissue (skin and subcutaneous fat). The aim of this study was to test this experimentally *in vivo* in measurements on human muscle.

The anisotropy of the light propagation has already been shown in human skin (Nickell *et al* 2000) and in dentin (Kienle *et al* 2003). More interesting for our purposes, Marquez *et al* (1998) have shown that this phenomenon exists *in vitro* on the chicken breast tissue. However, to our knowledge, no measurements have until now been performed on humans.

To measure anisotropy it is necessary to have a model against which to ‘fit’ the optical data. The first general theoretical approach was proposed by Heino *et al* (2002) following which several papers have now been published allowing anisotropy to be estimated from experimental data. Most of this work is based on the theory of the continuous-time random walk (Weiss 1994) and can take into account different tissues geometries and anisotropy orientations (Dagdug *et al* 2003, Dudko *et al* 2004, Hebden *et al* 2004, Dudko and Weiss 2005). In this present work we have used the methods proposed by Dagdug *et al* (2003), the advantage being that the validity of this approach has already been tested successfully on calibrated phantoms (Hebden *et al* 2004). This theory explicitly characterizes the anisotropy in terms of a bias parameter B defined as the ratio of the transition probabilities in directions parallel and perpendicular to the muscle fibres. Thus, the aim of the present work was to assess the parameter B for the skeletal muscle of a group of subjects and to see if there is any variability in this parameter among the different subjects. The parameter B is assessed by fitting the time-dispersion curves of the reflected photons travelling in the human *biceps brachii* using the Dagdug *et al* (2003) model (see methods section).

2. Material and methods

2.1. Subjects

The measurements were performed on 16 (12 males and 4 females) healthy subjects (age 34.8 ± 9.2 years, body weight 72.3 ± 12.4 kg, height 1.77 ± 0.08 m). The adipose tissue thickness (ATT) of the subjects at the point of measurement was distributed over the range 1.5–9.7 mm.

2.2. The choice of the muscle

The choice of the muscle was made with the aim of it having a simple morphological structure, allowing in this way the use of a simple and reliable model for the assessment of the anisotropy parameter B . The majority of the human skeletal muscles are pennated, which means that the direction of the fibres does not follow the direction of the muscle contraction and the pennation angle may continuously change over short distances (i.e. centimetres). This means that it may be difficult to know in advance the angle that the fibres form with the skin surface. We must also not neglect the fact that the pennation angle can change among subjects with joint position or with the intensity of muscle contraction (Narici *et al* 1996, Binzoni *et al* 2001). Such a situation would require the use of a complex model taking into account all the necessary degrees of freedom, making it much more difficult to estimate B through a fitting procedure. Moreover, many muscles are situated at a considerable distance below the skin surface and thus cannot be monitored by the NIRS technique. For this reason, if we want to overcome all these difficulties, choice of muscle group to study becomes very restricted and this is the reason why the *biceps brachii* has been chosen. In fact, as shown in figure 1 the *biceps brachii* lies just under the skin surface and the muscle fibres are parallel to it, following the direction of the *humerus*. These conditions remain the same for all subjects and are independent of age, joint position, cross section size, etc. Prior knowledge of this geometry allows us to use a very simple model to analyse the results (see below).

2.3. Experimental protocol

The dispersion curves of the photons travelling through the human *biceps brachii* were obtained as a function of wavelength, by using a femto-second time-resolved spectrometer (Abrahamsson *et al* 2004). The data were stored as 512×512 images with one axis

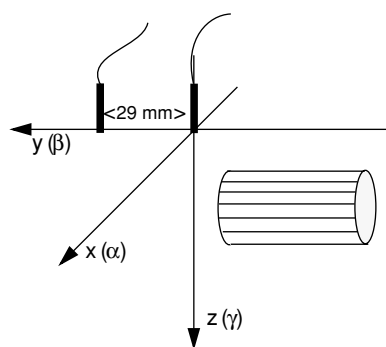


Figure 2. Schematic diagram of the optode positions (thick vertical bars separated by 29 mm) with respect to the investigated muscle, and defining the Cartesian axis for equation (1). The zero coordinate origin (0, 0, 0) is given by the intersection of the axes. The striated cylinder represents the muscle fibre direction (along the y-axis). The skin surface is given by the x - y plane and the muscle extends over a semi-infinite half space where z has positive values. The parameters α , β and γ are the transition probabilities for a photon to travel along the x , y , and z axis, respectively (positive and negative directions are assumed equiprobable).

corresponding to the time-dispersion and the other to the wavelength (see the following sections). The subject was asked to sit comfortably with the right forearm lying in a horizontal plane situated at heart level. The *radius* was positioned normal to the coronal plane of the subject and the arm was slightly distended (elbow angle $\approx 145^\circ$). The two optodes (source and detector), connected via two optical fibres to the spectrometer setup, were fixed through two holes, at 29 mm separation, on a rigid rectangular black support with the ends of the optodes protruding slightly (1 mm) from the support face. The optodes were then centred along the medial line of the short head of the right *biceps brachii*, at the point where the muscle transverse cross section is the largest. The support holding the two optodes was then securely fixed on the skin surface by means of medical adhesive tape. In this configuration the optodes were normal to the skin surface and aligned along the direction of the muscle fibres (see figure 2). The data acquisition was performed in the dark to eliminate any possible influence of the laboratory illumination on the measurements. One image was acquired for each subject and the acquisition time for one image was 4.11 min (11 subjects) and 3.52 min (5 subjects). Immediately after the first image a reference image was also acquired (see section 3.7). In this case, the optodes (source and detector) were placed directly facing each other, separated by an appropriate neutral density filter in order to obtain an appropriate light intensity. The instrumental parameters were the same as those used to obtain the first image. A detailed description of the spectrometer setup which is based on Abrahamsson *et al* (2004) is given in the following sections (see also figure 3 and table 1).

2.4. Light source

Broadband picosecond pulses were generated by using a photonic crystal fibre combined with a femtosecond mode locked Ti:sapphire laser. The laser provided <100 fs pulses at a 79.536 MHz repetition rate, with a wavelength set to 800 nm. The actual power utilized for the present application was set to $0.85 \text{ W} \pm 0.02 \text{ W}$. A small fraction ($\sim 4\%$) of this light was split off to a photodiode using a microscope glass slide and used for synchronization. An optical isolator was used after the laser to prevent optical reflections causing unstable optical output conditions. The light output from the isolator was focused into the crystal fibre by using

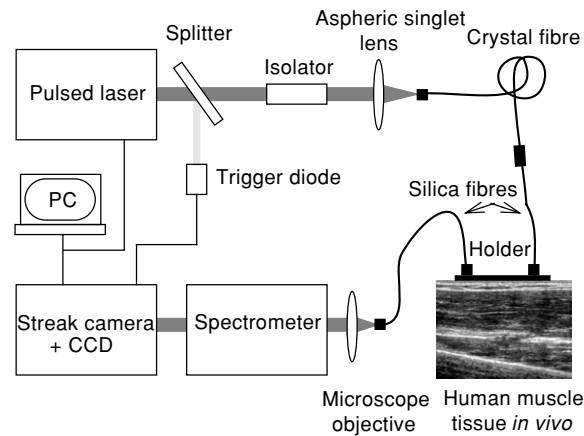


Figure 3. Spectrometer setup. The characteristics of the different components are listed in table 1.

Table 1. Characteristics of the different components composing the spectrometer setup of figure 3.

	Technical information (see also the text)	Company
Pulsed laser	Max power at 800 nm: 0.97 mW	MAI TAI, Spectra Physics, Mountain View, CA, USA
Optical isolator	Set for a wavelength of 800 nm	I-80-T4, ISOWAVE, Dover, NJ, USA
Aspheric singlet lens		GelTech® C150TM-B, Thorlabs GmbH, Karslfed, Germany
Crystal fibre	Pure silica crystal fibre, holes distributed in a hexagonal geometry, 1 m long, core diameter of 1.8 μm , cladding diameter of 120 μm , buffer cladding diameter 240 μm , numerical aperture of 0.38. The zero dispersion wavelength was 750 nm	NL.PM.750, Crystal Fiber A/S, Copenhagen, Denmark
Silica fibre (source)	Core diameter of 50 μm , cladding diameter of 125 μm , buffer cladding diameter of 900 μm , numerical aperture of 0.22	SEDI Fibres Optiques, Courcouronnes, France
Silica fibre (detector)	Core diameter of 300 μm , cladding diameter of 2 mm, buffer for the cladding diameter of 3 mm, numerical aperture of 0.37	SEDI Fibres Optiques, Courcouronnes, France
Spectrometer	50 grooves mm^{-1} grating blazed at 600 nm, entrance aperture set to 50 μm	250 IS, Chromex
Microscope objective lens	$\times 10$; numerical aperture of 0.25	Edmund Optics, USA
Streak camera	Equipped with a S20 streak tube	C5680, Hamamatsu, Japan
CCD camera		C4742-95-12ER, Hamamatsu, Japan

an aspheric singlet lens. The extremities of the crystal fibre were terminated with FC/APC type connectors and the end facets were sealed to prevent potential destruction of the fibre at high laser power e.g. through unwanted dust deposition. One connector was then mounted on a three axis optical alignment mount allowing the precise alignment of the crystal fibre with the laser beam. The light from the crystal fibre was then guided to the subject with a

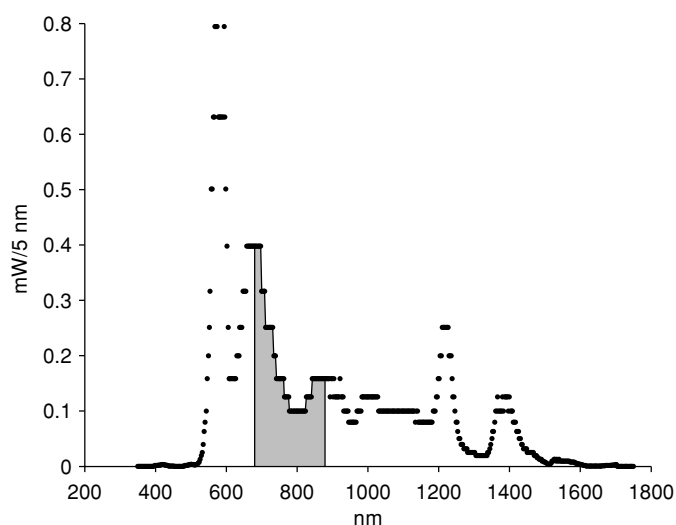


Figure 4. Mean power of the supercontinuum pulses generated at the tip of the crystal fibre reported as a function of the wavelength. Each point is the mean power over a range of 5 nm around the given wavelength (the total power for all the wavelengths is ~ 53 mW). The grey region represents the wavelength range actually utilized in the present investigation, i.e. at the end of the detection chain (680–880 nm).

1 m long silica fibre. The extremities of the fibre were again terminated with FC/PC type connectors. At the subject end of the fibre a collimating lens was directly mounted on the connector, resulting in an optode generating a collimated beam of 2 mm diameter. In practice, picosecond super continuum pulses were generated directly in the crystal fibre thanks to the combination of several nonlinear phenomena such as high order soliton formation, stimulated Raman scattering and four wave mixing (Ranka *et al* 2000, Coen *et al* 2002, Genty *et al* 2002). Figure 4 shows the mean power of the spectrum generated by the crystal fibre as a function of the wavelength and was acquired with an optical spectrum analyser (MS9710C, Anritsu, Tokyo, Japan) set to a resolution of 5 nm. The region highlighted in grey represents the wavelength range used in the present investigation (i.e. 680–880 nm).

2.5. Detection chain

The light coming from the subject was collected using a 1 m long silica fibre. The fibre end in contact with the subject was terminated with a metallic ferrule allowing it to be fixed in the black support and, the other end was terminated with a FC/PC type connector. The light was then focalized on a spectrometer using a conventional microscope objective. The spectrally dispersed light was captured by a streak camera operating in the synchro-scan mode (i.e. allowing it to collect all the light pulses). At the end of the acquisition chain the time resolved spectra were captured by a CCD camera. The black level was subtracted after each acquisition before the data were stored on the hard disk of a PC.

2.6. Spectrometer setup calibration

The spectrometer wavelength scale was calibrated using a series of wavelengths in 5 nm steps directly generated by the MAI TAI tunable laser. The total spectral range was 671.56 to 917.18 nm and a resolution of 0.48 nm per pixel.

The calibration of the time scale for each wavelength was performed by separating the optodes by known amounts using a calibrated metallic rail. The resulting differences in the travel times of the pulses were measured and compared to the known displacements. This resulted in a time scale axis varying from 0 to a maximum value between 1.88 and 1.91 ns, depending on the wavelength.

The response of the system to intensity was calibrated by using a series of optical density filters which had previously been calibrated by using a white source (Filament lamp, Leybold Optics GmbH, Alzenau, Germany) and a portable spectrometer (USB2000, Ocean Optics BV, Duiven, The Netherlands). The calibrations were performed using the same parameter settings of the time resolved spectrometer that were used during the experimental protocol.

2.7. Evaluation of the possible optical anisotropy

Typically, one cannot directly analyse a given time-dispersion curve (i.e. the intensity of one row of the corresponding image as a function of the time axis) without first correcting for the instrumental response (i.e. it is necessary to deconvolve the time-dispersion curve with the reference signal) and, in this instance a Wiener filter based algorithm was used (Gonzalez and Woods 1992). Following this operation, the optical anisotropy of the tissue was estimated in the following way: for a given subject, the bias parameter B describing the eventual anisotropy of the light propagation in the skeletal muscle (see below) was calculated by fitting the measured time-dispersion curves with the mathematical model proposed by Dagdug *et al* (2003):

$$I_{\text{image}}(y, t) = AI(y, t) = A \frac{(B + 2)^{3/2}}{(2\pi)^{3/2} B^{1/2} (\mu'_s c (t - t_0))^{5/2}} \times \exp \left\{ - \left(\frac{1}{B} + \frac{1}{2} \right) \left[B + \left(\frac{y}{\sqrt{2}} \mu'_s \right)^2 \right] \frac{1}{\mu'_s c (t - t_0)} - \mu_a c (t - t_0) \right\} \quad (1)$$

where $I(y, t)$ is the intensity of the photon flux, for a given wavelength, proportional to the image intensity, $I_{\text{image}}(y, t)$. The parameters y , A , c , t and t_0 are the interoptode distance, a proportionality constant, the speed of light in the tissue ($2.14 \times 10^2 \text{ mm ns}^{-1}$ with an index of refraction $n = 1.4$), the time variable and a time constant defining the zero time. As explained, in Dagdug *et al* (2003) the bias parameter B allows one to compute the probabilities α , β and γ for a photon to move in one direction along the x , y and z axis, respectively, i.e.:

$$\alpha = \gamma = \frac{1}{2B + 4} \quad (2)$$

and

$$\beta = \frac{B}{2B + 4}. \quad (3)$$

The correspondence between the probabilities and the axis for two subjects are shown in figure 5 and by definition one has $2\alpha + 2\beta + 2\gamma = 1$ (i.e. there is the same probability of going in the positive or in the negative direction along the axes). The relations $\alpha = \gamma \neq \beta$ result from the symmetry of the morphological structure of the investigated muscle (i.e. the human *biceps brachii* fibres are parallel to the skin surface shown as in figure 1) and the position of the optodes. The fitting parameters A , t_0 , μ_a , μ'_s and B were estimated with a Levenberg–Marquart algorithm and by including the constraints $A \geq 0$, $\mu_a > 0$, $\mu'_s > 0$ and $B \geq 0$. The presence of the time parameter t_0 is due to the fact that time-dispersion curve and reference are not acquired simultaneously and this obliges us to restart two times the acquisition and thus the trigger, giving in this way two slightly different ‘zero times’. One typical mean value for t_0 is $\sim -0.057 \text{ ns}$. An independent fitting was performed for each wavelength obtaining in this way

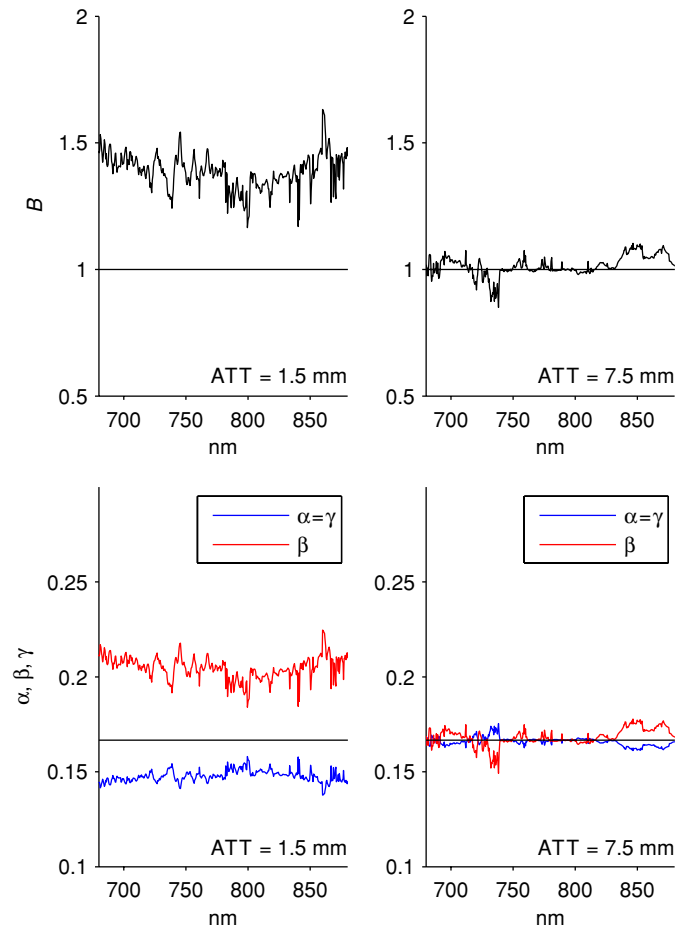


Figure 5. The bias parameter B and transition probabilities α , β and γ for two subjects, as a function of the wavelength. One subject has an adipose tissue thickness (ATT) of 1.5 mm (graphs on the left) and the other 7.5 mm. The parameter B defines the level of anisotropy for the propagation of the photons in the muscle. A value $B = 1$ means that the tissue is perfectly isotropic (black horizontal line). The parameters α , β and γ are the transition probabilities for a photon to travel along the x , y and z axis, respectively, and are computed from B (equations (2) and (3)). The value $\alpha = \beta = \gamma = 1/6$ means that the tissue is perfectly isotropic.

several B values. This analysis was repeated for each subject. Given that the sensitivity of the time resolved spectrometer setup was low for the extreme wavelength values, only the data falling in the range 680–880 nm were analysed (corresponding to the grey region in figure 4).

3. Results

The upper figures in figure 5 show the calculated B values as a function of the investigated wavelength range for two subjects with different ATT. A value of B equal to 1 means that the medium, in this case the tissue, is perfectly isotropic. In figure 5 (lower figures) are the corresponding α , β and γ values obtained using equations (2) and (3). The black horizontal

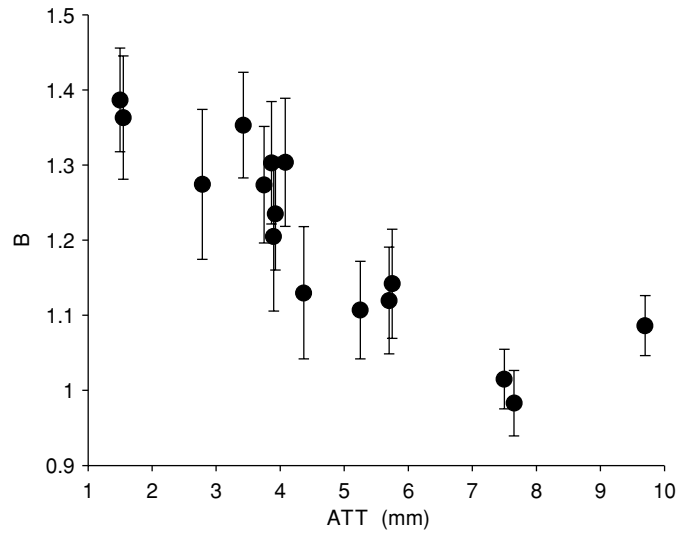


Figure 6. Mean of the bias parameter B values taken over the range 680–880 nm as a function of the adipose tissue thickness (ATT). The vertical bars correspond to the standard deviation. Each filled circle represents a different subject.

line corresponds in this case to a probability of $\alpha = \beta = \gamma = 1/6$, i.e. the photons have the same probability of going in any direction along the x , y and z axes. No particular dependence of B , and as a consequence of α , β and γ , on the wavelength has been observed by analysing all the group subjects. We are not aware of any theoretical model that has yet been developed against which to describe these observations. For this reason, to examine the global behaviour of B , figure 6 shows the mean values of the parameter B computed over the investigated wavelength range (see e.g. figure 5), as a function of the ATT, i.e. each point corresponds to a different subject. From figure 6 one can see that as the ATT becomes larger then B decreases and tends to the value 1.

Figure 7 reports the mean values (computed over the investigated wavelength range) of the α , β and γ probabilities, as a function of ATT. It is possible to observe from figure 7 that the probabilities tend to the value of $1/6$ (i.e. $\sim 0.33/2$) as ATT increases, i.e. the value for which $\alpha = \beta = \gamma$. Figure 7 also shows that when the ATT values are small, then $\beta > \alpha = \gamma$. This means that in this instance the probability for a photon to travel along the direction of the muscle fibres is greater than the probability of it travelling perpendicular to them. For small ATT values, α and γ have a value of ~ 0.15 and $\beta \sim 0.2$.

4. Discussion

The present results clearly show that the propagation of photons in the human *biceps brachii* is anisotropic. In fact one can see in figure 7 that, for small ATT, the probability of a photon travelling along the fibre direction (y -axis) is higher than of it travelling in the perpendicular direction. Any contribution of the *brachialis* muscle (see figure 1) to the B value results should be small because it is situated deep under the skin; moreover, the orientation of its fibres is not very different from that of the *biceps brachii*. The present results are consistent with the findings obtained *in vitro* on chicken breast (Marquez *et al* 1998) and with Monte Carlo simulations where in the latter case the muscle fibres are represented by oriented cylinders

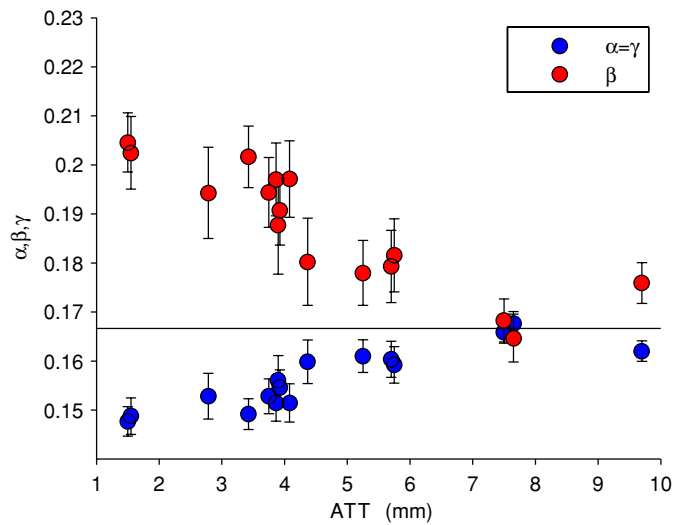


Figure 7. Mean of the transition probabilities α , β and γ , representing the probability of a photon travelling along the x , y and z axis, respectively. The mean is taken over the range 680–880 nm and plotted as a function of the adipose tissue thickness (ATT). The vertical bars correspond to the standard deviation. Each pair of red and blue circles, for the same ATT, represents a different subject. The probabilities α , β and γ are computed from the B data (before averaging) in figure 6.

(Kienle *et al* 2004). The interesting point here, is that thanks to the model represented by equation (1), the parameter B represents the anisotropy generated by the ‘cylindrical’ geometry of the muscle fibres, whilst the ‘anisotropy’ of the general scatterers distributed in the medium (described for instance by a Henyey–Greenstein phase function) is always included in the usual transport-corrected scattering coefficient (Kienle *et al* 2003). Thus, the parameter B allows us to investigate independently the effect of the macroscopic morphological structure of the muscle.

From the data appearing in figure 7 we can also observe that when ATT increases, the anisotropy is completely lost because all the probabilities tend to the value $1/6$ (horizontal black line). This phenomenon is probably explained by the fact that when the ATT becomes large, the light travels preferentially in the adipose tissue and that the contribution of the muscle to the time-dispersion curve becomes negligible. Since the adipose tissue (hypodermis) has no precise oriented structure (i.e. the cells are not long fibres as in the case of the muscle), when the ATT is large the anisotropy is completely lost.

Thus, the present results may be summarized by saying that the probability for a photon to travel along the direction of the muscle fibres is higher ($\sim 0.2 + \sim 0.2 = 0.4$, i.e. for the positive and negative directions on the y -axis) than that of travelling along a perpendicular axis ($\sim 0.15 + \sim 0.15 = 0.3$, i.e. for the positive and negative directions on the x or z axis) while in the adipose tissue the probability is the same ($\sim 0.33/2 + \sim 0.33/2 = 0.33$) in all directions (see figures 7 and 4).

Of course, to better investigate this problem it will be necessary in the future to develop a model taking into account the presence of many different layers of tissue. It is also true that the epidermis/dermis layer is also anisotropic for the photon propagation (Nickell *et al* 2000). However, the contribution of epidermis and the dermis to the ATT thickness is of the order of ~ 1 mm and this does not vary greatly between subjects. So given that in this instance the interoptode spacing was very large compared to the thickness of this layer, it is not surprising

that B appears not to be sensitive to the effects of this layer. (The probability for light travelling inside this ~ 1 mm layer situated on the surface is very small compared to the probability of it travelling in the rest of the investigated tissue volume).

In conclusion, the present study highlights the fact that when performing experimental studies on skeletal muscle metabolism using NIRS, it is important not to neglect the possible influence of the architecture of the muscular tissue on the measured parameters. This is especially true when using NIRS instrumentation that does not allow the estimation of all optical variables (e.g. as is the case with simple single channel continuous wave spectrometers). If the effects of muscle anisotropy are ignored, this may influence derived physiological quantities such as haemoglobin oxygen saturation, oxygen consumption, etc. With respect to this last point, the present results are compatible with and can explain in part the observations made by Miura *et al* (2004) and Quaresima *et al* (2001) where the authors observed different haemoglobin saturation and oxygen consumption values in different regions of the human, the *gastrocnemius medialis*, the *vastus lateralis* and the *rectus femoris*. These muscles have different and varying fibre fascicle orientation. Interestingly, Miura *et al* (2004) have shown a correlation between these physiological values and the pennation angle of the muscle in these particular regions. Of course, the orientation of the muscle fibres might not be the only reason for the observed inhomogeneities in the human skeletal muscle, and indeed we have shown that blood vessel distribution (especially the presence of perforator vessels) might also contribute to this phenomenon (Binzoni *et al* 2004), but, in this latter case, the variations must be interpreted as real physiological differences and not as optical artefacts.

Acknowledgments

We thank Hamamatsu, Japan and France, for the loan of the streak camera and the spectrometer. We would like also to thank Dr German Abdo (Département Radiologie et informatique médicale, Geneva, Switzerland), for the ultrasound image shown in figure 1.

References

- Abrahamsson C, Svensson T, Svanberg S, Andersson-Engels S, Johansson J and Folestad S 2004 Time and wavelength resolved spectroscopy of turbid media using light continuum generated in a crystal fiber *Opt. Express* **12** 4103–12
- Arridge S R, Cope M and Delpy D T 1992 The theoretical basis for the determination of optical pathlength in tissue: temporal and frequency analysis *Phys. Med. Biol.* **37** 1531–60
- Binzoni T, Bianchi S, Hanquinet S, Kaelin A, Sayegh Y, Dumont M and Jequier S 2001 Human gastrocnemius medialis pennation angle as a function of age: from newborn to the elderly *J. Physiol. Anthropol. Appl. Hum. Sci.* **20** 293–8
- Binzoni T, Leung T, Delpy D T, Fauci M A and Rufenacht D 2004 Mapping human skeletal muscle perforator vessels using a quantum well infrared photodetector (QWIP) might explain the variability of NIRS and LDF measurements *Phys. Med. Biol.* **49** N165–73
- Binzoni T, Ngo L, Hiltbrand E, Springett R and Delpy D 2002 Non-standard O₂ consumption-temperature curves during rest and isometric exercise in human skeletal muscle *Comp. Biochem. Physiol. A Mol. Integr. Physiol.* **132** 27–32
- Coen S, Chau A H L, Leonhardt R, Harvey J D, Knight J C, Wadsworth W J and Russell P S J 2002 Supercontinuum generation by stimulated Raman scattering and parametric four-wave mixing in photonic crystal fibers *J. Opt. Am. Soc. Am. B* **19** 753–64
- Dagdug L, Weiss G H and Gandjbakhche A H 2003 Effects of anisotropic optical properties on photon migration in structured tissues *Phys. Med. Biol.* **48** 1361–70
- Delpy D T and Cope M 1997 Quantification in tissue near-infrared spectroscopy *Philos. Trans. R. Soc. Lond. B Biol. Sci.* **352** 649–59

- Dudko O K and Weiss G H 2005 Estimation of anisotropic optical parameters of tissue in a slab geometry *Biophys. J.* **88** 3205–11
- Dudko O K, Weiss G H, Chernomordik V and Gandjbakhche A H 2004 Photon migration in turbid media with anisotropic optical properties *Phys. Med. Biol.* **49** 3979–89
- Ferrari M, Binzoni T and Quaresima V 1997 Oxidative metabolism in muscle *Philos. Trans. R. Soc. Lond. B Biol. Sci.* **352** 677–83
- Ferrari M, Mottola L and Quaresima V 2004 Principles, techniques, and limitations of near infrared spectroscopy *Can. J. Appl. Physiol.* **29** 4634–87
- Genty G, Lehtonen M, Ludvigsen H, Broeng J and Kaivola M 2002 Spectral broadening of femtosecond pulses into continuum radiation in microstructured fibers *Opt. Express* **10** 1083–98
- Gonzalez R C and Woods R E 1992 *Digital Image Processing* (Reading, MA: Addison-Wesley)
- Hebden J C, Guerrero J J, Chernomordik V and Gandjbakhche A H 2004 Experimental evaluation of an anisotropic scattering model of a slab geometry *Opt. Lett.* **29** 2518–20
- Heino J, Arridge S and Sommersalo E 2002 Anisotropic effect in light scattering and some implications in optical tomography *Tech. Dig. OSA Biomedical Topical Meetings* pp 18–20
- Kienle A, Forster F K, Diebold R and Hibst R 2003 Light propagation in dentin: influence of microstructure on anisotropy *Phys. Med. Biol.* **48** N7–N14
- Kienle A, Forster F K and Hibst R 2004 Anisotropy of light propagation in biological tissue *Opt. Lett.* **29** 2617–9
- Marchesini R 1999 Comments on the paper 'Optical properties of bovine muscle tissue *in vitro*; a comparison of methods' *Phys. Med. Biol.* **44** L7–8
- Marquez G, Wang L H V, Lin S P, Schwartz J A and Thomsen S L 1998 Anisotropy in the absorption and scattering spectra of chicken breast tissue *Appl. Opt.* **37** 798–804
- Martelli F, Sassaroli A, Yamada Y and Zaccanti G 2002 Analytical approximate solutions of the time-domain diffusion equation in layered slabs *J. Opt. Soc. Am. A Opt. Image Sci. Vis.* **19** 71–80
- Miura H, McCully K, Nioka S and Chance B 2004 Relationship between muscle architectural features and oxygenation status determined by near infrared device *Eur. J. Appl. Physiol.* **91** 273–8
- Narici M V, Binzoni T, Hiltbrand E, Fasel J, Terrier F and Cerretelli P 1996 In vivo human gastrocnemius architecture with changing joint angle at rest and during graded isometric contraction *J. Physiol.* **496** 287–97
- Nickell S, Hermann M, Essenpreis M, Farrell T J, Kramer U and Patterson M S 2000 Anisotropy of light propagation in human skin *Phys. Med. Biol.* **45** 2873–86
- Quaresima V, Colier W N, van der Sluijs M and Ferrari M 2001 Nonuniform quadriceps O₂ consumption revealed by near infrared multipoint measurements *Biochem. Biophys. Res. Commun.* **285** 1034–9
- Ranka J K, Windeler R S and Stentz A J 2000 Visible continuum generation in air-silica microstructure optical fibers with anomalous dispersion at 800 nm *Opt. Lett.* **25** 25–7
- Weiss G H 1994 *Aspects and Applications of the Random Walk* (Amsterdam: North-Holland)
- Zijp J R and ter Bosch J J 1998 Optical properties of bovine muscle tissue *in vitro*; a comparison of methods *Phys. Med. Biol.* **43** 3065–81